U.S. Department of Commerce
National Oceanic and Atmospheric Administration
National Weather Service
National Centers for Environmental Prediction
5830 University Research Court
College Park, MD 20740-3818

Office Note 496
https://doi.org/10.25923/d9rn-fd18

MÖBIUS NET CUBED-SPHERE GNOMONIC GRIDS

R. James Purser*
IM Systems Group, Rockville, Maryland

September 26, 2018

* email: jim.purser@noaa.gov

Abstract

A 'gnomomic grid' on the spherical surface is one whose grid lines are great circles and therefore centrally project as straight lines in a plane tangent to the sphere. For a cubed-sphere, a gnomonic grid on each face projects onto the plane tangent to the sphere at the center of the face to form a net of orthogonal lines on this plane. Each one of the two families of lines associated with a given face corresponds to the family of planes they belong to that share an axis of mutual intersection through the center of the sphere. The angular distribution of these planes at this shared axis can be chosen to define a characteristic type of gnomonic cubed grid. For the purposes of atmospheric numerical modeling and data assimilation, the most natural choice is to have the planes defining the grid lines to be equally-spaced in angle (the 'equiangular' gnomonic cube grid). With this convenient choice, the problem of interpolating from the grid to targets located close to a cube-edge is a relatively simple one because the family of lines of which the edge is a member is smoothly continued in passing from one face to its neighbor. Thus, extrapolating the grid of one face needed to supply a sufficient margin for subsequent centered-stencil interpolations to arbitrary target points in that cube's face involves only one-dimensional interpolations to generate the extra needed grid points. However, the equiangular gnomonic grid is not the only one possessing this property. By a minor adjustment to the angular spacing of the grid lines of each family, it is possible to make all three families of grid lines shared by the three faces that meet at a cube-corner engage in perfect three-way intersections in the vicinity of that corner. This is analogous to the construction of a 'Möbius net' configuration of lines in classical projective geometry. When a form of grid has this property one obtains further simplification of the subsequent interpolations, especially when broad stencils are desired. A proposed method of constructing such a Möbius-net gnomonic cubed sphere grid is described.

1. Introduction

Since the pioneering work of Sadourny (1972), but especially in the more recent period corresponding to the emergence of massive paraellization as the dominant computing paradigm for large scale atmospheric modeling, the importance and convenience of the cubed-sphere grid architecture for the horizontal numerical framework of global models has been generally recognized. A central, or 'gnomonic', radial projection between a sphere and a concentric cube provides the simplest class. We shall refer to these generically as the *gnomonic* types of the cubed-sphere grids provided the grid lines projected onto the surface of the cubes are straight and parallel to edges, forming a net of orthogonal lines. This implies that the grid lines on the sphere are great circles. In Sadourny's study, the grid was constructed such that the lines were equidistantly spaced on the surface of the cube, which unfortunately implies a noticeable excessive crowding of the projected great circle grid lines on the sphere near the cube edges, which can lead to numerical inefficiency. But a higher implied resolution near edges is not always entirely a disadvantage given that the numerical truncation errors of finite difference schemes near edge discontinuities are often greater, other things being equal, and the extra resolution there tends consequently to compensate.

Another natural choice of gnomonic grid type, strongly advocated by Ronchi et al. (1996), has the grid lines of each family equally spaced in angle. In this case, which has become known as the 'equiangular' gnomonic grid, as opposed to Sadourny's original 'equidistant' grid, the resolution on the sphere is much more uniform. Fig. 1 shows both the equidistant and equiangular grids at very low resolution, where the more uniform resolution of the equiangular case, panel (b), compared to the equidistant form, panel (a), is evident. However, as already noted above, and confirmed in the comparative study of Rančić et al. (1996), the equiangular grid is not necessarily an improvement as judged by how it affects the numerical accuracy of solutions.

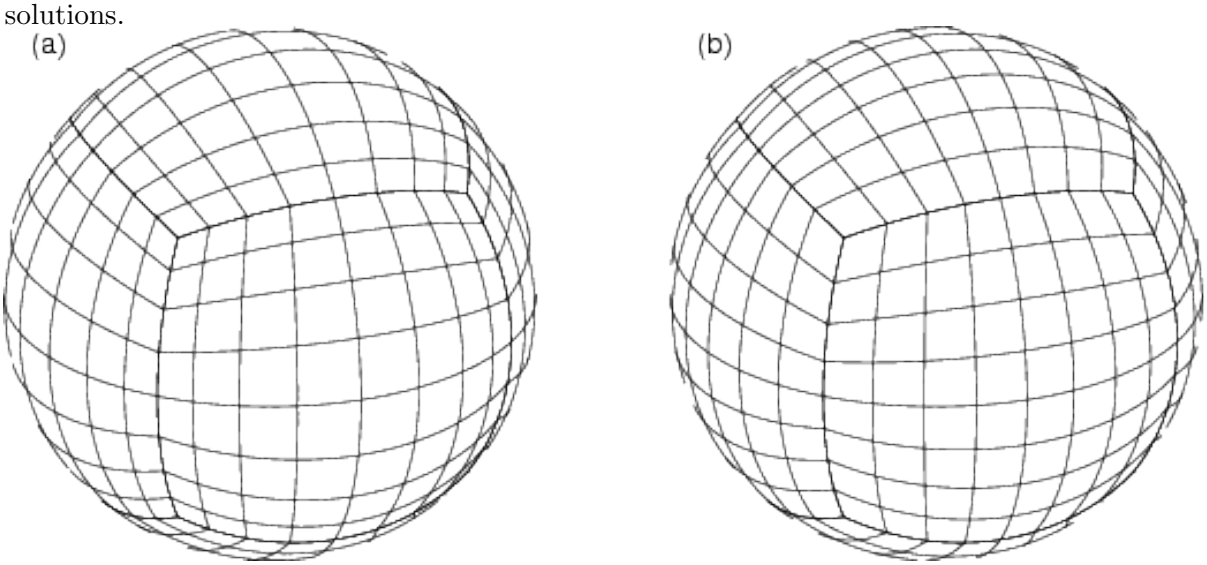

Figure 1. (a) The 'equidistant' gnomonic grid, which is very far from being of uniform resolution on the sphere, and (b) the 'equiangular' gnomonic grid, which is relatively more uniform in its resolution on the sphere.

The main practical advantage that Ronchi et al. emphasized is that the equiangular family of grid lines of one cube face smoothly continue their uniform progression past each cube-edge (which also belongs to this family) to merge with the family of grid lines of the contiguous face; this is not true of the equidistant form of the grid as the overlap at a cube-edge illustrated in Fig. 2a clearly shows. But the equiangular grid, whose corresponding overlap is illustrated in Fig. 2b, and in Fig. 4 of Ronchi et al. (1996), enjoys a perfect coincidence of these overlapping grid lines. This means that the reconciliation of the overlapping solutions of a model at each time step entails only *one*-dimensional interpolations (in the direction parallel to the shared grid lines), implying significant gains in computational efficiency as well as a streamlining of computer code compared to other general composite mesh methods (Starius, 1980; Browning et al., 1989) and most other gnomonic cubed sphere grids.

There are other types of the gnomonic cubed sphere grids. For example, the FV3 cubed sphere model, based on the earlier work of Lin and Rood (1997) and Putman and Lin (2007), which is scheduled for imminent operational use as the next-generation global forecast model at NCEP, presently uses a grid intermediate between the equidistant and equiangular forms (in a sense that we make precise in Appendix A), such that the spacing of grid points along the *edges* of the cube is uniform. This configuration shares with the equidistant grid the aforementioned

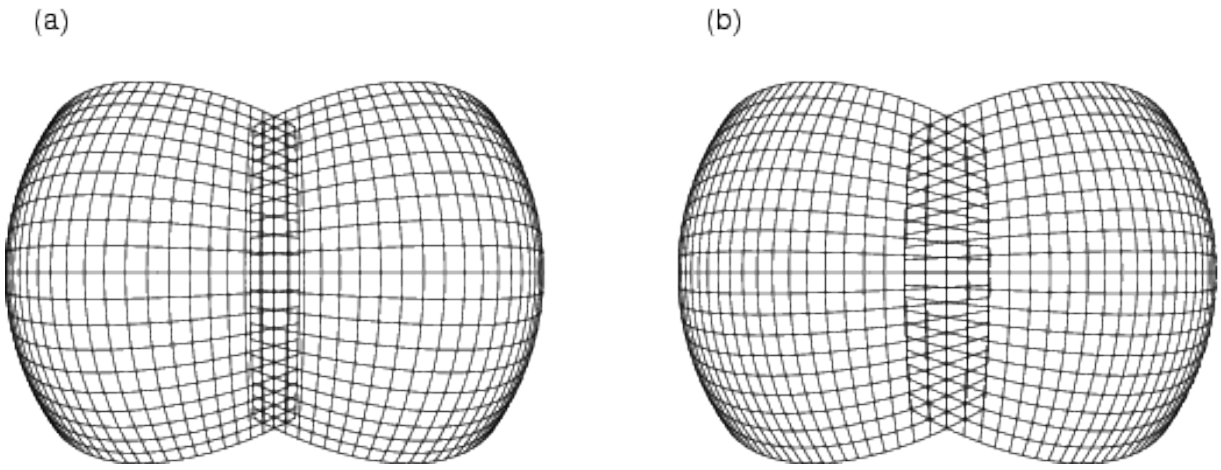

Figure 2. (a) The equidistant gnomonic grid's edge overlap, shown in the style of Fig. 4 of Ronchi et al. (1996), for a pair of contiguous faces, showing that the extended grid's lines do not coincide with those of the neighboring face of the cube for this type of gnomonic grid. (b) The equivalent figure for the equiangular gnomonic grid, showing that the grid lines of the extended grid in the overlap *do* coincide exactly with the grid lines of the neighboring face in this case.

disadvantage that the preparation of an extended grid beyond the edges of the cube requires two-dimensional interpolation.

We should not suppose that the equiangular is the only possible gnomonic grid that benefits from the numerical convenience of having smoothly coinciding families of grid lines when extended and overlapped beyond the cube edges. Moreover, if one is interested only in fully unstaggered grids (which is often the case in tasks associated with data assimilation) and if we then pay attention to the regions in the vicinity of the two cube corners that terminate the edge where the two overlapping grids are shown, it is strikingly clear in Fig 2b that the points of the extended portion of each grid in the overlap region are each extremely close to a corresponding point that belongs to the native grid of this neighboring tile. Therefore, only a tiny perturbation in the definition of the grid would be needed to make these points coincide and, if this can be arranged in a smooth and consistent way, all of the problems associated with interpolation from our cubed-sphere grid become very much simpler (especially when the overlap regions are relatively wide and the interpolation stencils are relatively broad).

The central projection onto any plane of any gnomonic grid from the sphere must, by definition, result in a grid composed only of straight lines. But a special case of the problem of constructing grids of straight lines possessing three-way exact intersections also arises in the realm of classical projective geometry, particularly in its relation to the representation by a perspective transformation of a uniform tiling on one plane as it would appear projected by straight 'lines of sight' through ordinary space onto another plane. In this form, the resulting geometrical construction is known as a 'Möbius net'. It turns out that the problem we need to solve is a slightly generalized form of this classical geometrical idea, and we will devote section 2 to a discussion of the relevant aspects of projective geometry to show exactly how the construction of the Möbius net can be generalized in the way that satisfies our requirements. However, in its ideal analytic form, the resulting Möbius net grid is only practical near the corners of the cube because, as the Möbius net grid lines get closer to the medians of the cube faces, these grid lines pack progressively closer together and become infinite in number with the

cube-face median as a limit. In order to formulate a practical grid we must therefore smoothly graft between the usable Möbius net strips of the grid lines of each family, centered on the cube edges where they behave well, an alternative distribution of the grid lines starting some finite distance away from these edges. Polynomial splines provide the obvious and natural way to 'fill in' the grid lines where the Möbius net would be too dense, as we explain in section 3. In fitting an interpolating spline of this kind, the index of the grid line is proportional to the polynomial in the angle made by the plane of the grid line with the median plane of the cube face that the spline largely spans. The polynomial is therefore an odd function of this angle (by symmetry) and its degree rises by two for every additional degree of continuity attained at the two 'joins' beyond which the Möbius net takes over. It is not obvious that the spline defined in this fashion should provide a monotonic grid for each degree of continuity and for each half-width of the Möbius zone; nevertheless, in Appendix B, we prove that this monotonicity property does indeed hold in the general case. The conclusions are given in Section 4.

2. Projective geometry

In projective geometry, ordinary points and lines are supplemented by 'ideal points' or 'points at infinity', and 'ideal lines' or 'lines at infinity'. These remove the need for certain complicating qualifications in generic statements about incidence among the members of the sets of lines and points. Such statements make up a substantial proportion of the content of projective geometry in its 'pure' form, which is concerned with properties of geometrical configurations that remain invariant under projective transformations. Good texts on projective geometry are provided by Seidenberg (1962) and Coxeter (1987), where the terminology and standard proofs are presented in detail.

The idea of a projective transformation generalizes that of a perspective transformation. That is, we consider the projective space to be just one of the possible hyperspaces embedded in an ordinary space of one extra dimension in which there is considered to be a point of perspective, not contained in our original 'source' space. From this point of perspective and the 'pencil' of straight rays or lines that pass through this point (are 'concurrent' through this point), we can map each point of the original embedded source space via such a line to a unique corresponding point on some other 'image hyperplane' that also does not contain the point of perspective; this defines a perspective transformation between our original source space and the image space, including the ideal points, that are associated with the orientations of the special rays parallel to the source or image spaces. Unlike an optical projection, where there is a directionality to each light ray, in a perspective transformation of projective geometry, the locations of the two intersections of the ray or line with the source and image spaces need not be on one particular side, or even on the same side, of the point of perspective.

The 'projective transformations' are those mappings that can be factored into a finite number of perspective transformations. They map points to points, and lines to lines, and some source or image points and lines may be of the ideal variety. Projective transformations do not preserve angles and do not preserve distances, although when a configuration comprises many angles and line segments, certain functions among several angles and some ratios of several line segments may be found to be preserved by projective transformations.

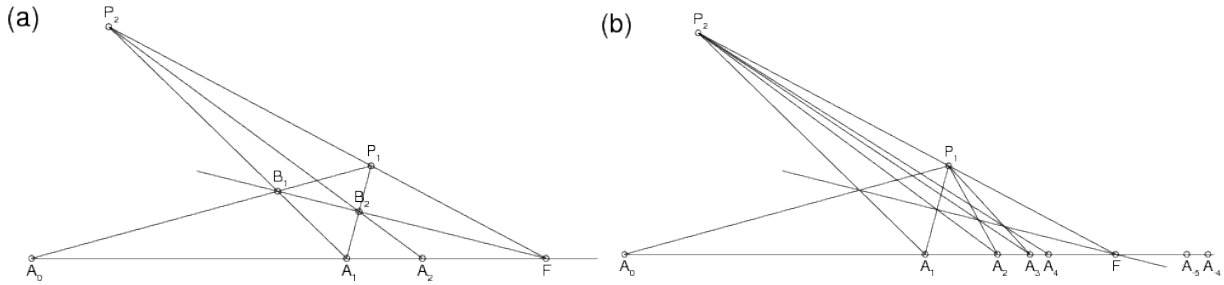

Figure 3. A harmonic net of points, A_n, constructed by projective transformations on a line with one fixed point, F. Two projection points, P_1 and P_2, are collinear with F and serve to project the points, A_n, onto corresponding points, B_n, along another line through F in the manner shown by the initial construction (a), and then extended iteratively, (b), to fill in further members of the sequence, A_n. The distances, A_nF, form a doubly-infinite harmonic sequence.

Fig. 3a illustrates a construction of a special form of one-dimensional projective transformation from points on the line, A_0F, back into the same line. This is accomplished by taking a perspective transformation from each A_n to the point, B_n, on another line intersecting the original through a point, F, using a point of perspective, P_1. Then a perspective transformation of this B_n using a second point of perspective, P_2, collinear with F and P_1, completes the projective transformation back onto the original line, A_0F, to the new point, A_{n+1}. Similarly, we can take the projective image of A_1 and call it A_2, or we can reverse the sense of the iterations. Therefore, when this process is repeated, we obtain what is called a 'harmonic net' or 'parabolic net' of points, A_n, which is doubly infinite, and we find that the directed (signed) distances, $r_n = |A_nF|$, form a harmonic sequence in the sense that $1/r_n - 1/r_{n+1} = K$, for some constant, K. As shown in the Fig. 3b, the sequence of points A_n extends for both positive and negative n with the net of points converging to the single 'fixed point', F (which remains unmoved by our projective transformation), from both sides of it.

The Möbius net, as it is traditionally introduced (see, for example, Fauvel et al., 1993) extends the idea of a harmonic net to two dimensions by the construction illustrated in Fig. 4. The harmonic nets are important historically in the role they played in the perspective art of uniform tilings, but they are not the most general forms of projective nets, even in one dimension. If the line on which the B points lie in Fig. 3a does *not* pass through the same point that joins P_2P_1 and A_0A_1, which we now call F_2, but instead intersects the line of points A at a distinct point, F_1, then we find that the one-dimensional net constructed by the previous construction now has *two* fixed points, F_1 and F_2. The net is as illustrated in the construction of Fig. 5a. If we place the origin at the center of the interval, F_1F_2, and denote the half-width of the interval by r_∞, then the points A_n within the interval bounded by the fixed points can be shown to follow the pattern,

$$r_n = r_\infty \tanh(\xi + n\gamma/2), \tag{2.1}$$

for some pair of parameters, ξ and γ, when both members of a consecutive pair lie inside the interval, or

$$r_n = r_\infty \coth(\xi + n\gamma/2), \tag{2.2}$$

when both members of a consecutive pair lie outside the interval (and with the same γ). However, when the intermediate line of projection (where the 'B' points reside) is straddled by the

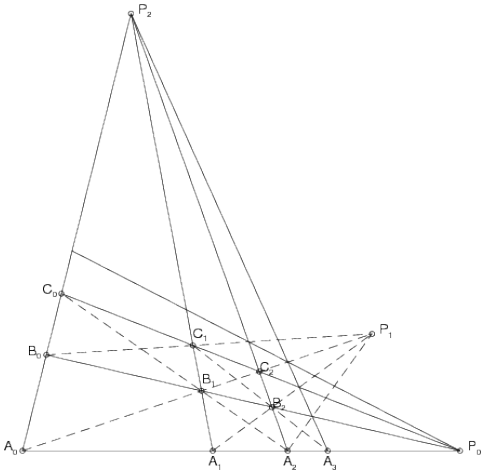

Figure 4. The construction of the Möbius net in its traditional form. Starting with a line containing distinct points A_0 and A_2 and a fixed perspective point, P_0, a second line through A_0 also containing point C_0 and a second fixed point of perspective, P_2, construct lines C_0P_0 and A_2P_2 intersecting at C_2. Let B_1 be the intersection of the two 'diagonals', A_0C_2 and A_2C_0, and let this point project from P_2 onto the point A_1 on A_0P_0, and project from P_0 onto the point, B_0, on A_0P_2. If we now form B_2 as the intersection of A_2P_2 and B_0P_0, and C_1 as the intersection of A_1P_2 and C_0P_0, we find that diagonals, such as A_1B_2, A_0B_1, and B_0C_1 are concurrent at a third fixed point, P_1, which lies on the same line as P_0 and P_2. A_0, A_1, A_2 and B_0, B_1, B_2 and C_0, C_1, C_2 form parts of projectively-equivalent harmonic sequencies converging towards P_0. To continue these sequences, first we define C_3 as the intersection of A_1P_1 and C_0P_0, and find corresponding B_3 and A_3 by the intersections of the line C_3P_2 with the lines B_0P_0 and A_0P_0 respectively. Similarly, we can continue harmonic sequences of the forms A_n, B_n, C_n and so on, converging towards P_2. The complete Möbius net constructed this way fills the plane (including the portion on the opposite side of the line of the fixed points, $P_0P_1P_2$ in this presentation).

projection points, P_1 and P_2, as shown in Fig. 5b, then the sequence of A_n alternates between the inside and outside of the interval, and then

$$r_n = \begin{cases} r_\infty \tanh(\xi + n\gamma/2) & : \quad n \text{ is even} \\ r_\infty \coth(\xi + n\gamma/2) & : \quad n \text{ is odd} \end{cases} . \tag{2.3}$$

A further possibility occurs when, with this alternating pattern, $A_2 = A_0$, a situation where it is said that the projective transformation is an 'involution'. Note that, when it is an involution for the mapping from some point, A_0, to A_1 (and vice versa), it is an involution for *every* point A on the line except F_1 and F_2. Obviously, in this case, we have $r_1 = r_\infty^2/r_0$. A_0 and A_1 are then an example of a '*conjugate pair*'.

In a projectively equivalent transformation of our line configurations to those where one of the fixed points becomes the ideal point at infinity, the distribution of distances r_n from the other fixed point, taken as the origin, behaves exponentially,

$$r_n = C(\pm 1)^n \exp(n\gamma), \tag{2.4}$$

where C is a positive constant and the exponentiated $+1$ or the -1 occurs according to whether consecutive points belong to the same, or the alternating, semi-infinite intervals. In the latter case, involution occurs when $\gamma = 0$. In the general case, the two constants, C and γ, as well as the disambiguation of the $\pm$ symbol, are determined once a consecutive pair of the sequence r_n is given.

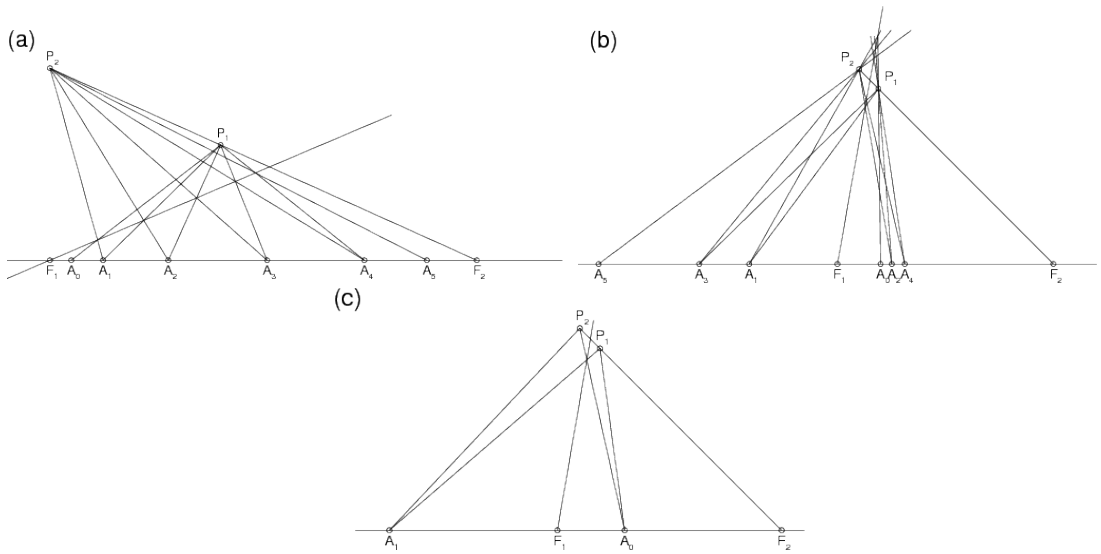

Figure 5. Construction of a one-dimensional hyperbolic net in an interval with two fixed points, F_1 and F_2. (a) The case with successive points falling within the same interval, with successive locations relative to the center of the interval given by a formula like Eq. (2.1). For points lying outside the interval (not shown), Eq. (2.2) would describe the sequence of locations. (b) The case showing a pattern of alternation of 'inside' and 'outside' locations of the A points with respect to the interval, where the locations relative to the center of the interval would be described by a formula like (2.3). (c) The case of an 'involution' in a one-dimensional projective transformation with two fixed points.

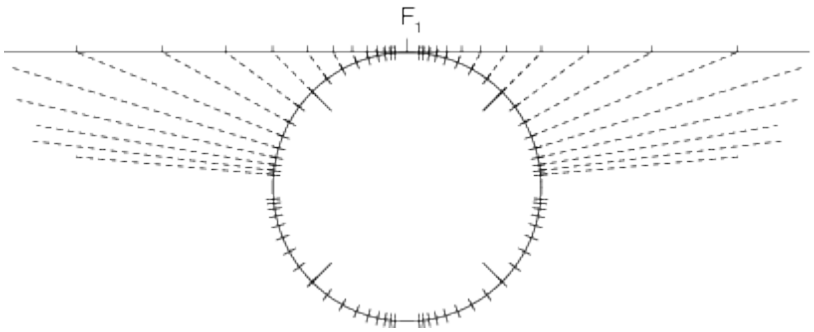

Figure 6. Schematic construction of the one-dimensional analog of the Möbius net grid on the circle using a gnomonic projection of a tangent plane inscribed with a hyperbolic net (and its involution, or mirror reflection about the finite fixed point, F_1). On the circle, the grid gains a new symmetry – it reflects into itself across the diagonal mirror-planes that mark the 'edges' of the four 'faces' of the squared-circle (analogous to the cubed sphere).

These harmonic and hyperbolic one-dimensional nets always display their simplest geometrical form when one fixed point is the ideal point; in the case of the harmonic net, the points then appear as an equally spaced sequence that is self-similar under translation; in the hyperbolical case, the net is self-similar under rescaling and, if all the conjugate points under the involution operation are included, the two intervals' grids are mirror images of each other across the origin. If we gnomonically project the harmonic net's uniform grid onto the unit circle, we obtain a one-dimensional version of the 'equidistant' gnomonic grid, which is not of interest to us. However, the projection onto the circle in the hyperbolic case where the net has the scaling

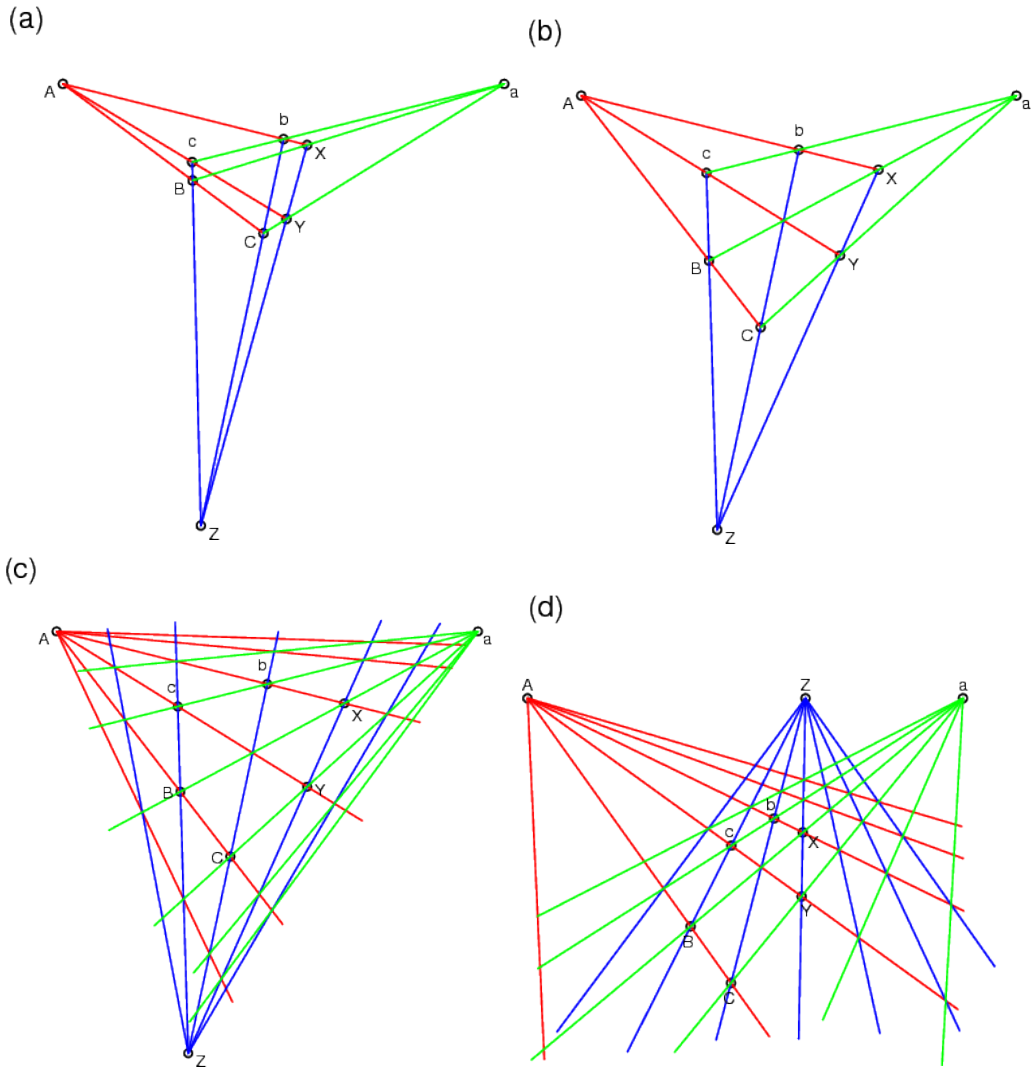

Figure 7. (a) The generic configuration illustrating the theorem of Pappus. Distinct points A, B and C are collinear; points a, b and c are also collinear. Opposite sides of the hexagon, $AcBaCb$, intersect at the three points X, Y, Z. The theorem states that X, Y and Z are then also collinear. (b) A small adjustment to the configuration of panel (a) that causes the lines AY, BX, and CZ to become concurrent in the center of the diagram. (c) By an iterative application of the theorem of Pappus we can extend the embryonic net of panel (b) to a more complete version that will eventually fill the triangle formed by the fixed points A, a and Z. The distributions of points along any given line of this net conform to the 'tanh' rule of (2.1) for one-dimensional hyperbolic projective transformations; the present construction is therefore just a natural extension into two dimensions of the concept of a projective hyperbolic net. (d) Like panel (c), but for the case where the three fixed points, A, a, and Z are coincident, in which case we recover the ordinary parabolic, or harmonic, form of the Möbius net.

self-similarity about the tangent point, F_1, leads to a grid on the circle with mirror symmetry also across the $\pm 45°$ diagonal axes, as illustated in Fig. 6. Thus we would obtain the same grid on the circle had we rotated the line containing the original grid by 90°, confirming that we trivially meet the criterion of grid coincidence in the overlaps of a 'gnomonic squared-circle' grid. We will see shortly how this 1D model generalizes to two (and even higher) dimensions,

but it is instructive to approach the problem in a projective-geometrical style first.

We take a fresh look at the construction of 2D nets by first presenting the generic case of the theorem in classical geometry of Pappus of Alexandria (Seidenberg, 1962), illustrated in Fig. 7a. Given three distinct collinear points, A, B, C, and another three distinct collinear points, a, b, c, we can form a hexagon, $AcBaCb$. Then the intersections, points X, Y and Z, of the lines of opposite sides of this hexagon are also collinear.

But it takes only a one-parameter generic variation of the set-up of this configuration to cause the lines AY, BX and CZ to become concurrent, as in Fig. 7b. By Brianchon's theorem (e.g., Coxeter 1987) this occurs when the hexagon $XYCBcb$ tangentially circumscribes an ellipse. When we extend the lines Zc, ZX, ac, aC, AX and AC, the additional intersections at our disposal allow us to apply Pappus's theorem again (repeatedly) to extend this net and hence to iteratively cover the interior of the triangle formed by the fixed points, A, a and Z. This is shown for a few of the next steps in Fig. 7c. To confirm that we are simply generalizing the more familiar parabolic or harmonic form of the Möbius net, we show the corresponding construction, with corresponding labels, in Fig. 7d for the special limiting case when the fixed points A, a, and Z are made collinear.

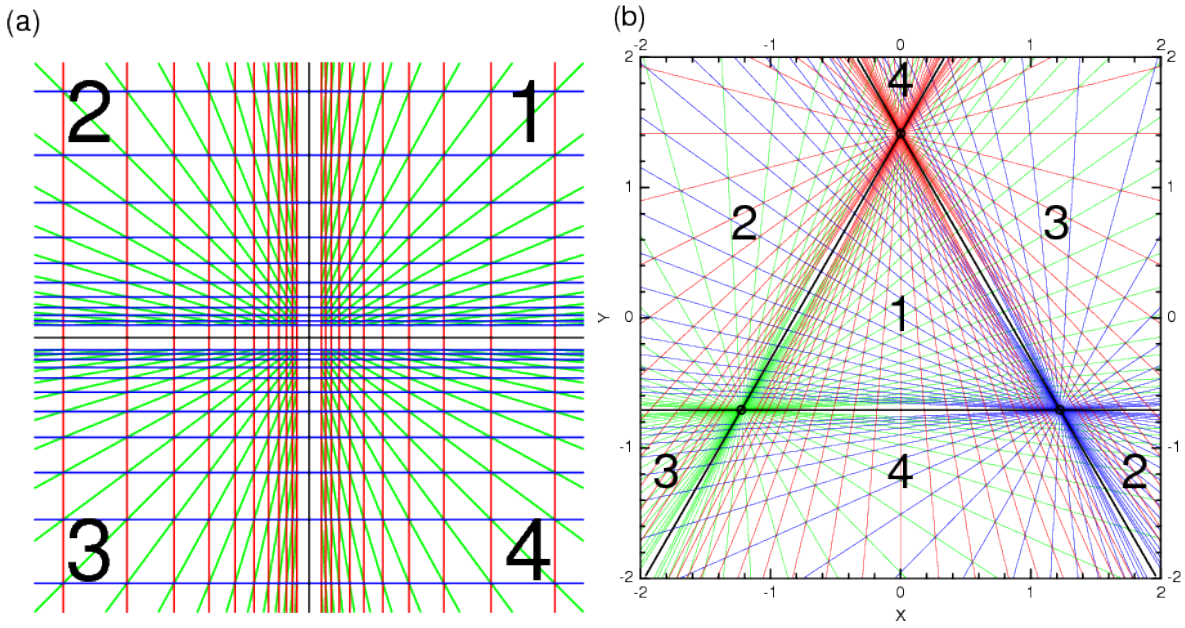

Figure 8. The hyperbolic Möbius net grid in its simplest and most symmetrical presentations: (a) when two of the fixed points are ideal and at orthogonal azimuth directions, in which case, the pattern of grid lines is invariant to a set of constant rescalings; (b) when all three fixed points lie on the vertices of an equilateral triangle. In the latter case, the chosen scaling corresponds in the case where the projective plane is considered tangent to the unit sphere in which is inscribed a regular octahedron whose edges now correspond, via gnomonic projection, to the triangle boundaries in the projective plane.

A generic 'triangle' of three nonconcurrent invariant lines in a 2D projective plane actually partitions the projective plane into four separate triangular regions. Amongst the hyperbolic projective transformations that fix the three vertices, there are now involutions that transpose the three sets of pairs of regions in such a way that any point in the interior of one of the

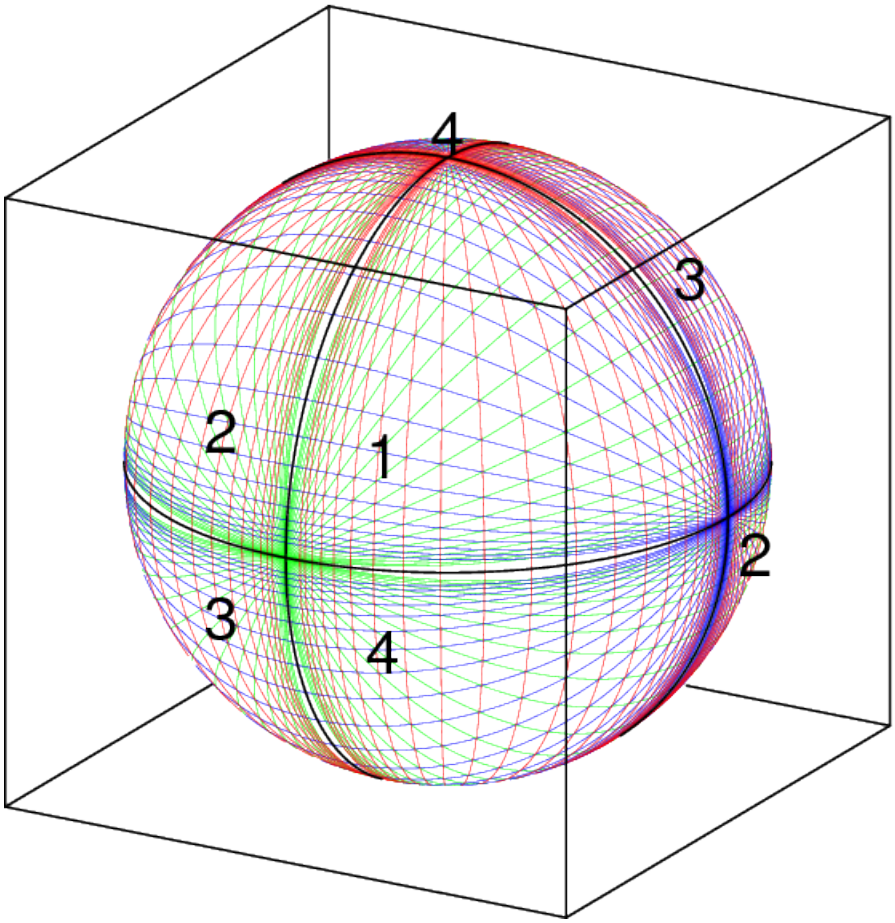

Figure 9. The same Möbius net of Fig. 8 centrally projected from the tangent planes onto the unit sphere, showing the octahedral symmetry. The bold great circles marking the projected octahedral edges, near which the grid becomes singular, correspond to the medians of the projected dual polyhedron, the cube. (The edges of the circumscribed cube are drawn here for reference.) Only the grid lines that pass through the middle portion of the triangular faces of the projected octahedron should be used in the construction of a practical gnomonic cubed-sphere grid, the rest of the grid needing to be filled in by a suitable interpolation.

triangles has a unique conjugate image in each of the other three regions, and hence, each hyperbolic net defined in one of the triangles has a unique image in each of the other regions. As should be clear from the 1D example of hyperbolic projective transformations, the simplest and most symmetrical presentation is achieved when we make all but one of the three fixed points 'ideal' and place this remaining one at the origin. If we further insist that the lines concurrent with the two fixed points at infinity are drawn in two perpendicular families in the representation's Cartesian coordinates, (X, Y), with grid lines in the first quadrant (following Eq. (2.4)) at $\hat{X}_i = \exp(\gamma_i)$ and $\hat{Y}_j = \exp(\gamma_j)$ as well as the fan of lines concurrent through the center of the form:

$$\frac{Y_j}{X_i} = \exp(\gamma(j - i)), \tag{2.5}$$

we obtain the symmetric presentation shown in Fig. 8a. If we rotate the sphere to make

the tangent point in the gnomonic projection correspond to a corner of the cube, or the face-center of the associated dual octahedron, we obtain another symmetrical configuration of Fig. 8b. (The four triangular regions into which the projective plane is partitioned by the three invariant lines are boldly numbered 1 through 4 in this figure.)

When this configuration is inscribed on the tangent plane $Z = 1$ of the unit sphere centered at $(X, Y, Z) = (0, 0, 0)$, and the gnomonic projection used to project the lines onto both hemispheres, we have defined the gnomonic Möbius net grid of nominal resolution γ. The result, shown in Fig. 9, has octahedral (or cubic) symmetry and exhibits the desired perfect three-way intersections at the eight corners of the cube dual to the octahedron of eight spherical triangles that are each filled by a copy of the projected single-triangle net.

All that remains is to decide how the regions of the grid away from the cube corners need to be replaced in order to preserve the good qualities while disposing of the chaotic bunching of the lines that lie close to the medians of the cube's faces.

3. Practical construction of the Möbius-net gnomonic cube grid

In order to make a practical global grid that preserves the desirable properties of the Möbius net in the corner regions of the cube, we need to keep the distribution of the final grid angles measured from the cube edges exactly in proportion to the corresponding angles given by the pure Möbius net projected back onto the sphere, in the symmetric way shown in Fig. 9, only within some small specified angle α; if this half-width of the 'Möbius zone' becomes too large, then we will see excessive bunching of our grid lines as we approach the median of each tile of the cube and the grid will cease to be useful. But with a small or modest width to the Möbius zone we can 'fill in' the central portion of our succession of grid lines between the two bounding zones by an appropriate smooth interpolation that preserves the continuity of the first few of the derivatives of the 'index variable' (a variable everywhere proportional to the index or coordinate label of the final grid) with respect to the true angle measured from the cube-tile median. Let us define this true angle to be ϕ, so that the cube-edges occur at $\phi = \pm\pi/4$, let the inner limits of the two associated Möbius zones occur at $\phi = \pm\phi_t \equiv \pm(\pi/4 - \alpha)$. Also, let us name the index variable, a, which we assume, once it is normalized, to range from -1 to $+1$ between the two cube-edges.

Based on the fact that the projected index variable, a, must conform locally to the distribution implied by (2.4) in the two Möbius zones where $|\phi| \geq \phi_t$, and attain ± 1 at $\phi = \pm\pi/4$, we deduce that, for a positive constant K, the two mutually-inverse relations must hold:

$$\phi(a) = \mp\frac{\pi}{4} + \frac{1}{2}\mathrm{gd}\left(\frac{a \pm 1}{K}\right), \quad \mp\phi \geq \phi_t \tag{3.1a}$$

$$a(\phi) = \mp 1 + K\,\mathrm{gd}^{-1}(2\phi \pm \pi/2), \quad \mp\phi \geq \phi_t, \tag{3.1b}$$

where the Gudermannian function, gd, and its functional inverse, gd^{-1}, are defined (e.g., Abramowitz and Stegun 1972, p77):

$$\mathrm{gd}(x) = \int_0^x \frac{1}{\cosh(t)}dt = 2\arctan(\tanh(x/2)) = 2\arctan(\exp(x)) - \pi/2 \tag{3.2a}$$

$$\mathrm{gd}^{-1}(y) = \int_0^y \frac{1}{\cos(t)}dt = 2\mathrm{arctanh}(\tan(y/2)) \equiv \ln\left[\tan\left(\frac{y}{2} + \frac{\pi}{4}\right)\right]. \tag{3.2b}$$

We do not initially know the calibrating constant, K, but our choice of method for filling in the distribution of $a(\phi)$ when $|\phi| \le \phi_t$ will end up fixing K.

The solution is to smoothly interpolate the index function $a(\phi)$ with a polynomial between the inner edges, located at $\phi = \pm\phi_t$, of the two Möbius zones. We do the interpolation using a polynomial 'spline' of degree $2n-1$ antisymmetric about the origin (i.e., odd powers of ϕ only), and a corresponding choice of the constant K, such that the value, and the first n derivatives, of the polynomial at these locations matches the corresponding values obtained from the inverse-Gudermannian based solutions that apply within the Möbius zones.

Denote the value of $a(\phi_t)$ by $1 + KA_0$, and its successive derivatives, which we wish to fit there, by KA_k, $k = 1, \ldots, n$. Note that the A_k are defined analytically:

$$A_k = \begin{cases} \mathrm{gd}^{-1}(-2\alpha) & : \quad k = 0 \\ 2^k \frac{d^k}{dz^k} \mathrm{gd}^{-1}(z)\Big|_{-2\alpha} & : \quad k > 0 \end{cases} . \tag{3.3}$$

The odd- and even-order derivatives of $\mathrm{gd}^{-1}(z)$ are given, for $k \ge 0$, by:

$$\frac{d^{2k+1}\mathrm{gd}^{-1}(z)}{dz^{2k+1}} = \sum_{j=0}^{k} (-1)^{j+k} \frac{(2j)! T_{k,j}}{\cos^{2j+1}(z)}, \tag{3.4}$$

and

$$\frac{d^{2k+2}\mathrm{gd}^{-1}(z)}{dz^{2k+2}} = \sum_{j=0}^{k} (-1)^{j+k} \frac{(2j+1)! \sin(z) T_{k,j}}{\cos^{2j+2}(z)}, \tag{3.5}$$

where the integers coefficients $T_{k,j}$ are defined recursively:

$$T_{k,0} = 1 \tag{3.6a}$$

$$T_{k,j} = 0, \quad j > k \tag{3.6b}$$

$$T_{k,j} = T_{k-1,j-1} + (2j+1)^2 T_{k-1,j}, \quad k, j > 0. \tag{3.6c}$$

These $T_{k,j}$ belong to a class of what Riordan (1968, p. 217) calls 'central factorial numbers'. The first fews rows of a tabulation of them are given in Table 1 (while a more complete tabulation can be found, in a slightly different arrangement, in Table A008958 of the On-line Encyclopedia of Integer Sequences, https://oeis.org/A008958).

Define the interpolating spline in terms of its n odd-degree Taylor expansion coefficients:

$$a(\phi) = \sum_{k=1}^{n} b_k \frac{\phi^{2k-1}}{(2k-1)!}, \quad |\phi| < \phi_t. \tag{3.7}$$

Define the system matrix $M_{i,j}$, $\quad 0 \le i, j \le n$ to have the coefficients:

$$M_{i,j} = \begin{cases} -A_i & : \quad j = 0 \\ 0 & : \quad 0 < 2j \le i \\ \phi_t^{2j-i-1}/(2j-i-1)! & : \quad 2j > i \end{cases} . \tag{3.8}$$

TABLE 1. Table of the first few of the central factorial numbers related to the formulae for the derivatives of the inverse-Gudermannian

k	$j=0$	1	2	3	4	5
0	1					
1	1	1				
2	1	10	1			
3	1	91	35	1		
4	1	820	966	84	1	
5	1	7381	24970	5082	165	1

Form the $(n+1)$-vector of 'unknowns', $\hat{b}_k$, by augmenting the polynomial coefficients, b_k, with an extra zeroth element as follows:

$$\hat{b}_k = \begin{cases} K & : \quad k = 0 \\ \\ b_k & : \quad 0 < k \leq n \end{cases}, \tag{3.9}$$

so that K is included among the unknowns, and finally, define the right-hand-side vector, U_k, for the system:

$$U_k = \begin{cases} 1 & : \quad k = 0 \\ \\ 0 & : \quad 0 < k \leq n \end{cases}. \tag{3.10}$$

Then solving

$$\boldsymbol{M}\hat{\boldsymbol{b}} = \boldsymbol{U}, \tag{3.11}$$

provides the calibrating constant K and the Taylor series coefficients, b_k that we need to smoothly graft a spline portion of the grid definition to the Möbius net portion. An example of this system for the quintic polynomial spline gives us:

$$\begin{bmatrix} -A_0 & \phi_t & \phi_t^3/6 & \phi_t^5/120 \\ -A_1 & 1 & \phi_t^2/2 & \phi_t^4/24 \\ -A_2 & 0 & \phi_t & \phi_t^3/6 \\ -A_3 & 0 & 1 & \phi_t^2/2 \end{bmatrix} \begin{bmatrix} K \\ b_1 \\ b_2 \\ b_3 \end{bmatrix} = \begin{bmatrix} 1 \\ 0 \\ 0 \\ 0 \end{bmatrix}. \tag{3.12}$$

The examples where we have chosen a relatively large $\alpha = 10^\circ$ and $n = 1, 2, 3, 4$, are plotted as graphs of the resulting $a(\phi)$ in Fig 10. For smaller values of α (which might be more suitable

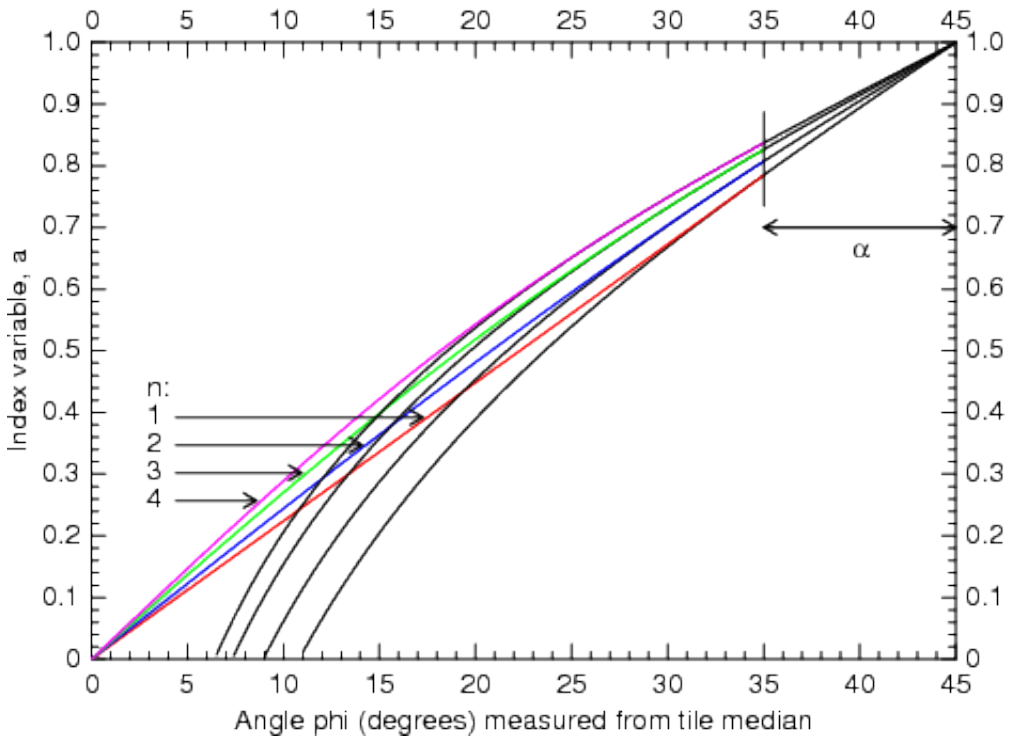

Figure 10. Examples of the graphs of the index variable, $a(\phi)$, plotted against the angle measured from the tile-median in the cases where the half-width of the Möbius zone is $\alpha = 10^\circ$ and the interpolating splines (colored curves) are of degrees $2n-1 = 1, 3, 5, 7$, corresponding to the continuity attained at the join, $\phi = 45^\circ - \alpha$, of degrees, $n = 1, 2, 3, 4$, respectively, as indicated by the arrows in the lower-left inset. The black curves are the graphs of the Möbius net $a(\phi)$ as defined by (3.1b) with the calibrating constants, K, needed to intercept the spline and match its first n derivatives at the join.

for the grids used in numerical models) it would become difficult to distinguish the resulting splines visually. While it is clear from the plotted graphs with these combinations of n and α that the interpolatory procedure gives rise to no unwanted oscillation, we might ask: is this the general case? To affirm that this is the case we state the following.

Theorem

For each positive $\alpha < \pi/4$ and for each odd degree interpolating spline, the function, $a(\phi)$, remains monotonic throughout the interval $\phi \in [-\pi/4, \pi/4]$.

□

The proof, which depends upon the properties of 'absolutely monotonic' functions (Bernstein, 1928; Widder, 1941) is provided in the Appendix B.

Figure 11 illustrates the construction of the Möbius net cubed sphere grid with order of continuity, $n = 1$, and a half-width of the Möbius zones of $\alpha = 11.75^\circ$. The grid in each tile is extended so as to cover (almost exactly) the surrounding Möbius zones. One can see that, within the hexagonal regions where three Möbius zones intersect, the desirable property of perfect three-way grid line intersections is achieved. In the Möbius zones just outside these hexagonal regions, it is not difficult to see examples of the failure of the three families of grid

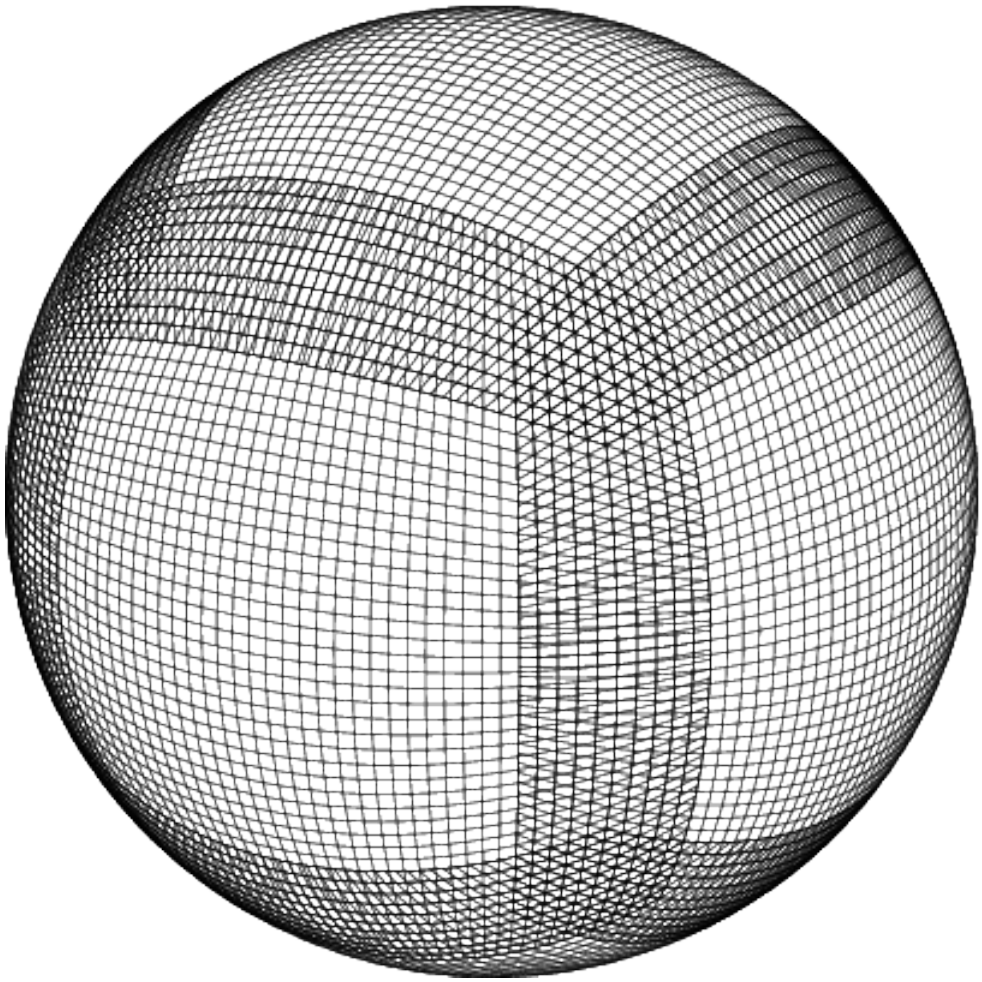

Figure 11. An example of a Möbius net cubed sphere grid with a degree of continuity, $n = 1$, and Möbius zones of half-width $\alpha = 11.75°$. The grid on each of the six cubic faces (tiles) is extended to almost exactly cover the surrounding Möbius zones, so that the perfect concurrence of the three families of grid lines within each of the hexagonal regions where three Möbius zones intersect can be visually verified.

lines to intersect concurrently.

This completes the detailed description and definition of this class of Möbius net gnomonic cubed sphere grids. Each form of the index function, $a(\phi)$, is completely defined by only two parameters: the index, n, that specifies the degree of continuity at the transition angles, $\phi = \pm\phi_t$, where the Möbius zones begin; and the angular half-width, α, of the Möbius zones.

4. Conclusions

We have exploited the ideas of classical projective geometry to show that there exists a class of gnomonic cubed sphere grids that enjoy the property exhibited by the traditional 'harmonic' and the more general 'hyperbolic' Möbius nets, that is, having coincident three-way intersections in regions of a prescribed size surrounding the cube-corners where this property is

most valuable. Polynomial splines are used to define the grid in the remaining area, so that the transition is as smooth as the polynomial degree allows, and it is shown that this guarantees monotonicity regardless of the location of the transition (implied by the angle α), or of the degree of the interpolating polynomial spline.

For a model, especially one employing a finite volume or element approach, the advantages of this new kind of gnomonic grid may not be significant in the course of the global model integration as there are no reasons to apply broad numerical stencils across the cube edges and corners. However, in other downstream applications, such as interpolating to nested subdomains, and especially in the problems of data assimilation where the numerical stencils associated with the manipulation of covariance operators may be very broad, then being able to have the points of the three adjoining grids extended across cube-corners coincide could be advantageous in terms of computational efficiency and in accommodating high-order spatial numerical operators in a streamlined way.

Acknowledgments

The author is grateful to Drs. Kristen Bathmann and Mark Iredell for their valuable reviews, and to Drs. Tom Black and Gerard Ketefian for stimulating discussions.

Appendix A

Geometry of a simple class of gnomonic grids

We focus on the specification of the grid lines of a tile centered on the point of zero latitude and longitude. It is always convenient to use Earth-centered Cartesian 3-vectors, scaled to give the Earth a unit-radius, when discussing questions of grid geometry on the sphere. To this end, we associate the Cartesian X-axis basis 3-vector, $\boldsymbol{E}_X = [1, 0, 0]$, with the equatorial point of zero longitude, and the Y-axis basis vector, $\boldsymbol{E}_Y = [0, 1, 0]$, with the equatorial point at longitude (measured east) 90°, and the intersection of the surface with Z-axis, the Cartesian 3-vector, $\boldsymbol{E}_Z = [0, 0, 1]$, at the North Pole. We need only define the latitude angles along the tile's median at longitude 0 (i.e., $Y = 0$) of each of the family of grid lines cutting this median perpendicularly and that contains an arc of the equator as a member; by cubic symmetry, all the other grid lines must follow a similar distribution. To our selected family of grid lines, we attach a map coordinate, y, with $y = 0$ denoting the equatorial arc, and $y = \pm 1$ denoting the bounding cube-edges, whose midpoints are at latitudes ±45°, or equivalently, at Cartesian $[1/\sqrt{2}, 0, \pm 1/\sqrt{2}]$.

We shall suppose that we wish the separation of the grid lines in this family to be uniform along the meridian at longitude $\pm\beta$ and that the latitude attained by a given grid line of this family at this longitude is η, while the latitude it attains along the central meridian, or median, of the tile, is θ. The crucial geometry of this situation is shown in two orthographic projections in Fig. 1, where, from the upper portion, we see by elementary trigonometry, that the elevation of the point on this grid line at the calibrating longitude, β, above the equatorial plane, $Z = 0$, is $h = \sin\eta$. But the tilted plane intersects the equatorial plane along the Y-axis, so, viewing the geometry along this line of sight, and referring to the corresponding lower portion of the

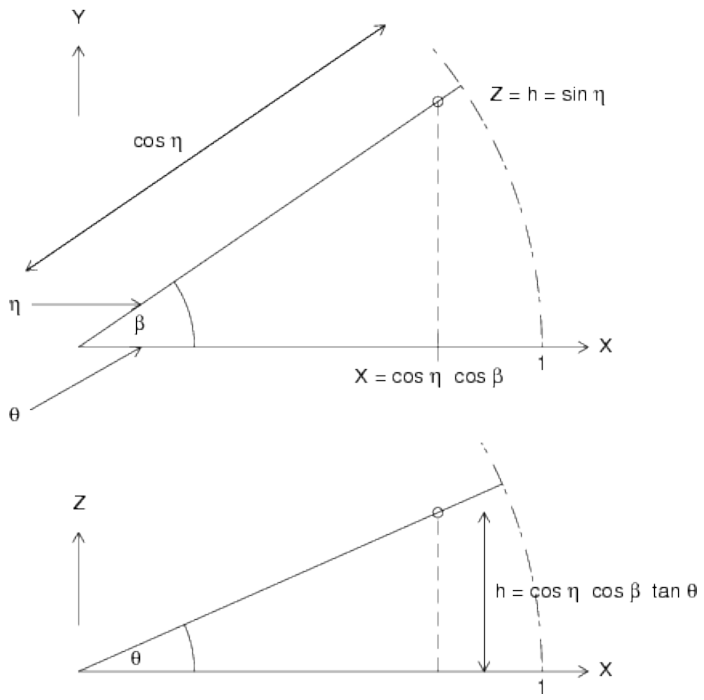

Figure A.1. The upper portion depicts a projection in the XY plane ($Z = 0$) of a contour at elevation above the equatorial plane h (dashed) of the tilted plane whose angle with the equatorial plane is η along the oblique line at longitude β, while in the XZ plane ($Y = 0$), the angle between the tilted plane and the equator is θ (the true angular separation of the planes). The lower portion depicts the same configuration projected in the XZ plane. θ is the maximum latitude attained by the gnomonic grid line that corresponds to the intersection of this tilted plane with the unit sphere (shown as the dot-dashed arcs).

figure where the XZ-plane projection is shown, we must also have that $h = \cos\eta \cos\beta \tan\theta$, and hence that

$$\theta = \arctan\left(\frac{\tan\eta}{\cos\beta}\right). \tag{A.1}$$

If $\hat{\eta}$ corresponds to the cube-edge, $\hat{\theta} = \pi/4$, where $y = 1$, then, since $\tan\hat{\theta} = 1$, we have:

$$\tan(\hat{\eta}) = \cos\beta. \tag{A.2}$$

Since we have chosen longitude β to be the one along which the latitudes η of the grid lines are equally spaced, we have

$$\eta = \hat{\eta} y, \tag{A.3}$$

and hence we can recover the true angle θ that the plane of the grid line at map coordinate y makes with the equatorial plane:

$$\theta = \arctan\left\{\frac{\tan[\arctan(B^{1/2})y]}{B^{1/2}}\right\}, \tag{A.4}$$

where

$$B = \cos^2\beta. \tag{A.5}$$

In the case $\beta = 0$, or $B = 1$, then

$$\theta = \frac{\pi y}{4}. \tag{A.6}$$

which is the just the equiangular case.

In the intermediate case, $\beta = \pi/4$, or $B = 1/2$, which is the choice presently employed in the FV3 cubed sphere,

$$\theta = \arctan\left\{\sqrt{2}\tan[\arctan(1/\sqrt{2})y]\right\}. \tag{A.7}$$

In the well-behaved extreme limit of maximum obliquity in the choice of calibrating longitude, $\beta \to \pi/2$, or $B \to 0$, we find that,

$$\theta = \arctan\{y\}, \tag{A.8}$$

which is simply another way of recovering the equidistant case of Sadourny (1972), showing that the present choice of grid in the FV3 model is indeed intermediate between the equiangular and equidistant forms of the gnomonic grid.

Finally, we remark that, although our convenient geometrical interpretation of the grid construction becomes obscured when $B > 1$ (the angle β thereby becoming imaginary) or $B < 0$ (imaginary $B^{1/2}$), this extended parameter range continues to provide valid and potentially useful members of this general family of gnomonic cubed sphere grids. Comparing the grid spacing at the cube-edge, $y = 1$, with that at the face-center, $y = 0$, we find:

$$\left.\frac{d\theta}{dy}\right|_{y=1} = \frac{(1+B)}{2}\left.\frac{d\theta}{dy}\right|_{y=0}. \tag{A.9}$$

But this means that a judicious choice of parameter, B, can be used to off-set the discrepancy of resolution between center and edge of a stand-alone nested grid when the nest is taken as a substantial portion of one face of the cube subjected to a transformation of either dilation or compression of the type proposed by Schmidt (1977)[†]. For example, when the Schmidt factor, s, is used to change the resolution of the grid at the center of the targeted face in accordance with the transformation,

$$\theta' = 2\arctan\left(\frac{\tan(\theta/2)}{s}\right), \tag{A.10}$$

then an equality of the resolution along the median line at the transformed edge-midpoint and at the face-center:

$$\left.\frac{d\theta'}{dy}\right|_{y=1} = \left.\frac{d\theta'}{dy}\right|_{y=0}, \tag{A.11}$$

is achieved when this transformation is combined with the parameter B of the gnomonic grid with the value:

$$B = \frac{1}{\sqrt{2}}\left(1 + \frac{\sqrt{2}-1}{s^2}\right). \tag{A.12}$$

[†] The idea for this application was stimulated by discussions the author had with Drs. Tom Black and Gerard Ketefian.

Appendix B

Proof of the monotonicity theorem of section 3

Definition

A function $f(z)$ is said to be **absolutely monotonic** in the interval, $a < z < b$, if it has non-negative value and derivatives of all orders there (Bernstein, 1928; Widder, 1941).

□

If a function is absolutely monotonic, then any positive integer power of the function defines another absolutely monotonic function.

The inverse-Gudermannian function $\mathrm{gd}^{-1}(z)$ is absolutely monotonic in the interval $0 < z < \pi/2$ because, expanded at the origin, its Taylor series coefficients (the absolute magnitudes of the Euler numbers) are all non-negative and the radius of convergence, $\pi/2$, spans the interval.

Likewise, the function, $\hat{y}(z) = 1 - \sqrt{1-z}$, is absolutely monotonic for $z \in [0, 1)$.

The approach to proving the montonicity theorem will be to show that the derivative, $da/d\phi$ of (3.1b), which is an even function about $\phi = 0$, must remain strictly positive when it is symmetrically interpolated by splines of even degree between the contact points at $\phi = \pm\phi_t, \quad 0 < \phi_t < \pi/4$, when the highest possible degree of continuity is imposed at these contact points.

First, we rescale the angle variable, $x = \phi/\phi_t$ so that the interval covered by the polynomial portion of the index function becomes simply $x \in [-1, 1]$. Define a symmetrical triangular hat function,

$$y(x) = 1 - |x|, \tag{B.1}$$

and a parabolic spline function,

$$z(x) = 1 - x^2, \tag{B.2}$$

and note that both functions vanish at $|x| = 1$ but have finite derivatives there. Since $z \le 1$ we can regard y as defining an implied function of z:

$$\hat{y}(z) \equiv y(x) = 1 - \sqrt{1 - z(x)}, \tag{B.3}$$

and, as we already noted above, $\hat{y}(z)$ is an example of an absolutely monotonic function in $[0, 1)$, so we can expand all positive powers of $\hat{y}$ in Taylor series with non-negative coefficients. Moreover, since $\hat{y}(0) = 0$, the first nonvanishing term in the expansion of $\hat{y}^k$ is the one in z^k, and therefore the matrix of the nonnegative coefficients $G_{k,j}$ in each of these expansions:

$$\hat{y}^k(z) = \sum_{j=0}^{\infty} \frac{G_{k,j}}{j!} z^j, \quad 0 \le z < 1, \tag{B.4}$$

is upper triangular,

$$G_{k,j} = 0, \quad j < k. \tag{B.5}$$

Also, since, $G_{0,0} = 1$, and

$$G_{1,j} = \frac{(2j-3)!!}{2^j} > 0, \quad j > 0, \tag{B.6}$$

if follows generally that,

$$G_{k,j} > 0, \quad j \geq k. \tag{B.7}$$

In the x coordinate, the derivative of the two displaced inverse-Gudermannian functions, i.e., secant functions centered on $x = \pm\pi/(4\phi_t)$ provides the analytic functional form (within a multiplicative constant) of the *density*, D, of the gnomonic grid coordinates defined purely by the Möbius net distributions on either side of $x = 0$:

$$D = \frac{1}{\cos(-2|x|\phi_t + \pi/2)}, \quad 0 < |x| < \frac{\pi}{2\phi_t}, \tag{B.8}$$

or equivalently, as an explicit function of y:

$$D(y) = \frac{1}{\cos(2(y\phi_t + \alpha))}, \quad -1 - \frac{2\alpha}{\phi_t} < y < 1, \tag{B.9}$$

which we also know to be positive, and an absolutely monotonic function (being the derivative of one) with respect to y in the subinterval, $0 \leq y < 1$. Let the successive derivatives of D with respect to y at $y = 0$ be D_k, which are non-negative by virtue of the absolute monotonicity:

$$D_k = \left.\frac{d^k D(y)}{dy^k}\right|_{y=0} \geq 0. \tag{B.10}$$

We can express function $D(y)$ as a Taylor-Maclaurin series about $y = 0$:

$$\begin{aligned} D(y) &= \sum_{k=0}^{\infty} \frac{D_k y^k}{k!} \\ &= \sum_{k=0}^{\infty} \sum_{j=k}^{\infty} \frac{D_k G_{k,j} z^j}{k! j!}, \end{aligned} \tag{B.11}$$

convergent for $|y| < 1$ (but obviously not at $y = 1$ corresponding to the median, $x = 0$ where D becomes infinite). The crucial observation is that, owing to $G_{k,j}$ being upper-triangular, the truncated series:

$$\hat{D}_n(y) = \sum_{k=0}^{n} \sum_{j=k}^{n} \frac{D_k G_{k,j} z^j}{k! j!}, \tag{B.12}$$

defines the desired polynomial spline since it already matches all derivatives of $D(y)$ up to order n at the pair of locations corresponding to $y = 0$, and is itself an even polynomial of the requisite degree, $2n$ in x. Moreover, $D_0 G_{0,0} = D(0) > 0$, and we have shown that the other terms in (B.12) are only non-negative multiples of each of the basis functions, z^j, which are themselves all positive in the interval $x \in (-1, 1)$. The implied positivity of the spline at all points in the interval proves the theorem.

References

Abramowitz, M., and I. A. Stegun — 1972 — *Handbook of Mathematical Functions with Formulas, Graphs, and Mathematical Tables.*, Dover, New York. 1046 pp.

Bernstein, S. N.	1928	Sur les functions absolument monotones. *Acta Mathematica,* **52,** 1–66.
Browning, G. L., J. J. Hack, and P. N. Swarztrauber	1989	A comparison of three numerical methods for solving differential equations on the sphere. *Mon. Wea. Rev.,* **117,** 1058–1075.
Coxeter, H. S. M.	1987	*Projective Geometry, 2nd Edition.* Springer, New York. 162 pp.
Fauvel, J., R. Wilson, and R. Flood	1993	*Möbius and his band; Mathematics and astronomy in nineteenth-century Germany.* Oxford University Press.
Lin, S.-J., and R. B. Rood	1997	An explicit flux-form semi-Lagrangian shallow water model on the sphere. *Quart. J. Roy. Meteor. Soc.,* **123,** 2477–2498.
Putman, W. M., and S.-J. Lin	2007	Finite-volume transport on various cubed-sphere grids. *J. Comput. Phys.,* **227,** 55–78.
Rančić, M., R. J. Purser, and F. Mesinger	1996	A global shallow-water model using an expanded spherical cube: Gnomonic versus conformal coordinates. *Quart. J. Roy. Meteor. Soc.,* **122,** 959–982.
Riordan, J.	1968	*Combinatorial Identities* Wiley, New York.
Sadourny, R.	1972	Conservative finite-differencing approximations of the primitive equations on quasi-uniform spherical grids. *Mon. Wea. Rev.,* **100,** 136–144.
Schmidt, F.	1977	Variable fine mesh in spectral global models. *Contrib. Atmos. Phys.,* **50,** 211–217.
Seidenberg, A.	1962	*Lectures in Projective Geometry.* Van Nostrand.
Starius, G.	1980	On composite mesh differencing methods for hyperbolic differential equations. *Numer. Math.* , **35,** 241–255.
Widder, D. V.	1941	*The Laplace Transform.* Princeton University Press. (Reprinted by Dover, 2010)